Fourier domain pump-probe optical coherence tomography imaging of Melanin

Desmond Jacob, Ryan L. Shelton, and Brian E. Applegate*

Department of Biomedical Engineering, Texas A&M University, 337 Zachry Engineering Center, College Station, TX 77843, USA.

**apple@tamu.edu*

Abstract: We report the development of a two-color Fourier domain Pump-Probe Optical Coherence Tomography (PPOCT) system. Tissue phantom experiments to characterize the system performance demonstrated imaging depths in excess of 725 μm, nearly comparable to the base Optical Coherence Tomography system. PPOCT A-line rates were also demonstrated in excess of 1 kHz. The physical origin of the PPOCT signal was investigated with a series of experiments which revealed that the signal is a mixture of short and long lifetime component signals. The short lifetime component was attributed to transient absorption while the long lifetime component may be due to a mixture of transient absorption and thermal effects. *Ex vivo* images of porcine iris demonstrated the potential for imaging melanin in the eye, where cancer of the melanocytes is the most common form of eye cancer in adults.

OCIS codes: (110.4500) Optical coherence tomography; (170.3880) Medical and biological imaging; (190.4180) Multiphoton processes.

References and links

1. D. Huang, E. A. Swanson, C. P. Lin, J. S. Schuman, W. G. Stinson, W. Chang, M. R. Hee, T. Flotte, K. Gregory, C. A. Puliafito, and J. G. Fujimoto, "Optical Coherence Tomography," Science **254**(5035), 1178–1181 (1991).
2. K. D. Rao, M. A. Choma, S. Yazdanfar, A. M. Rollins, and J. A. Izatt, "Molecular contrast in optical coherence tomography by use of a pump-probe technique," Opt. Lett. **28**(5), 340–342 (2003).
3. B. E. Applegate, and J. A. Izatt, "Molecular imaging of endogenous and exogenous chromophores using ground state recovery pump-probe optical coherence tomography," Opt. Express **14**(20), 9142–9155 (2006).
4. C. Yang, L. E. L. McGuckin, J. D. Simon, M. A. Choma, B. E. Applegate, and J. A. Izatt, "Spectral triangulation molecular contrast optical coherence tomography with indocyanine green as the contrast agent," Opt. Lett. **29**(17), 2016–2018 (2004).
5. D. J. Faber, E. G. Mik, M. C. G. Aalders, and T. G. van Leeuwen, "Toward assessment of blood oxygen saturation by spectroscopic optical coherence tomography," Opt. Lett. **30**(9), 1015–1017 (2005).
6. D. J. Faber, E. G. Mik, M. C. G. Aalders, and T. G. van Leeuwen, "Light absorption of (oxy-)hemoglobin assessed by spectroscopic optical coherence tomography," Opt. Lett. **28**(16), 1436–1438 (2003).
7. D. C. Adler, S. W. Huang, R. Huber, and J. G. Fujimoto, "Photothermal detection of gold nanoparticles using phase-sensitive optical coherence tomography," Opt. Express **16**(7), 4376–4393 (2008).
8. M. C. Skala, M. J. Crow, A. Wax, and J. A. Izatt, "Photothermal optical coherence tomography of Epidermal Growth Factor Receptor in Live Cells Using Immunotargeted Gold Nanospheres," Nano Lett. **8**(10), 3461–3467 (2008).
9. M. V. Sarunic, B. E. Applegate, and J. A. Izatt, "Spectral domain second-harmonic optical coherence tomography," Opt. Lett. **30**(18), 2391–2393 (2005).
10. B. E. Applegate, C. Yang, A. M. Rollins, and J. A. Izatt, "Polarization-resolved second-harmonic-generation optical coherence tomography in collagen," Opt. Lett. **29**(19), 2252–2254 (2004).
11. Y. Jiang, I. Tomov, Y. Wang, and Z. Chen, "Second-harmonic optical coherence tomography," Opt. Lett. **29**(10), 1090–1092 (2004).
12. J. S. Bredfeldt, C. Vinegoni, D. L. Marks, and S. A. Boppart, "Molecularly sensitive optical coherence tomography," Opt. Lett. **30**(5), 495–497 (2005).
13. D. L. Marks, and S. A. Boppart, "Nonlinear InterferometricVibrational Imaging," Phys. Rev. Lett. **92**(12), 1239051–1239054 (2004).

#125174 - $15.00 USD Received 8 Mar 2010; revised 11 May 2010; accepted 14 May 2010; published 26 May 2010

14. A. L. Oldenburg, B. E. Applegate, J. A. Izatt, and S. A. Boppart, "Molecular OCT Contrast Enhancement and Imaging," ″in *Optical Coherence Tomography: Technology and Applications*, W. Drexler, and J. G. Fujimoto, eds. (Springer, New York, 2009), pp. 713–752.
15. B. E. Applegate, C. Yang, and J. A. Izatt, "Theoretical comparison of the sensitivity of molecular contrast optical coherence tomography techniques," Opt. Express **13**(20), 8146–8163 (2005).
16. D. W. Kufe, J. F. Holland, E. Frei, and American Cancer Society., *Cancer medicine 6* (BC Decker, Hamilton, Ont.; Lewiston, NY, 2003).
17. J. Georges, and J. M. Mermet, "Thermal Lensing Spectroscopy - Principle and Applications," Analusis **16**, 203–215 (1988).
18. D. Schweitzer, S. Schenke, M. Hammer, F. Schweitzer, S. Jentsch, E. Birckner, W. Becker, and A. Bergmann, "Towards metabolic mapping of the human retina," Microsc. Res. Tech. **70**(5), 410–419 (2007).

1. Introduction

Optical Coherence Tomography (OCT) [1] is a non-contact imaging modality capable of micron scale resolution at depths of 1-2 mm in living tissue. OCT is used clinically for imaging the morphology of the retina and anterior segment of the eye. It is also finding new clinical applications, including intravascular imaging to identify vulnerable plaques. OCT inherently measures the backreflected tissue scattering and is therefore largely insensitive to particular molecular species residing in the tissue. The promise of molecular imaging with high resolution at these depths has spurred the adaptation of various molecular spectroscopy techniques to OCT, harnessing the power of physical phenomena such as light absorption [2–8], second harmonic generation [9–11], and coherent anti-Stokes Raman scattering [12, 13]. A consequence of the interferometric detection is that OCT is insensitive to incoherent phenomena such as fluorescence and Raman scattering. For a more detailed discussion of molecular contrast techniques in OCT see [14].

A previous theoretical analysis [15] of the potential sensitivity of various molecular spectroscopy techniques led to the identification of pump-probe spectroscopy as a promising route to molecular imaging with OCT. Based on that analysis a version of Pump-Probe OCT (PPOCT) called ground state recovery PPOCT [3] which probed the instantaneous changes in the ground state molecular population induced by the pump was developed. The prototype PPOCT system was based around a time-domain OCT system operating at 530 nm with degenerate pump and probe wavelengths. That system was successfully used to image concentrations of hemoglobin, dsRed, and rhodamine 6G. The filament arteries in Zebra danio fish were imaged *in situ* using the PPOCT signal from the hemoglobin in the erythrocytes. This work successfully demonstrated the practicality of achieving pump-probe spectroscopy based molecular imaging. However, there were several shortcomings, including slow line rates (~1 Hz) and limited penetration depth because of the short wavelength probe. The development of the current system was in part to address these shortcomings.

Hemoglobin and melanin are two of the most abundant chromophores in humans. The previously developed time-domain PPOCT system measured concentrations of hemoglobin. We have focused on melanin for the demonstration of this two-color Fourier domain PPOCT system. Melanin does not have a single molecular structure, but rather represents groups of molecules. There are three groups, eumelanin, pheomelanin, and neuoromelanin. Within each of these three groups are molecular species with different physical properties and biochemical functions. The different forms of melanin play various roles in the function of the brain, ear, eyes, and skin. There are a number of potential applications for a fast non-contact imaging technology which is capable of imaging melanin concentrations. One of the most important is as a tool to investigate and potentially diagnose melanoma, a particularly aggressive cancer starting in the melanocytes and the most common form of skin cancer. Melanoma originating in the uveal tract is also the most common cancer of the adult eye [16]. Obviously, biopsying any growth in the eye is problematic, hence a PPOCT technique sensitive to melanin could be an invaluable tool for the diagnosis and monitoring of eye melanomas.

Pump-probe spectroscopy fundamentally measures pump induced changes in the probe. The physical process which leads to the pump induced changes depends in part on the excited

#125174 - $15.00 USD Received 8 Mar 2010; revised 11 May 2010; accepted 14 May 2010; published 26 May 2010

state manifold of the molecule of interest. Most biomolecules have a complex network of electronic and vibrational excited states which comprise this manifold owing to their large size. Figure 1 is a partial electronic energy level diagram for a generic biomolecule illustrating some of the processes. Within this figure a number of spontaneous processes are indicated by dashed arrows, some of

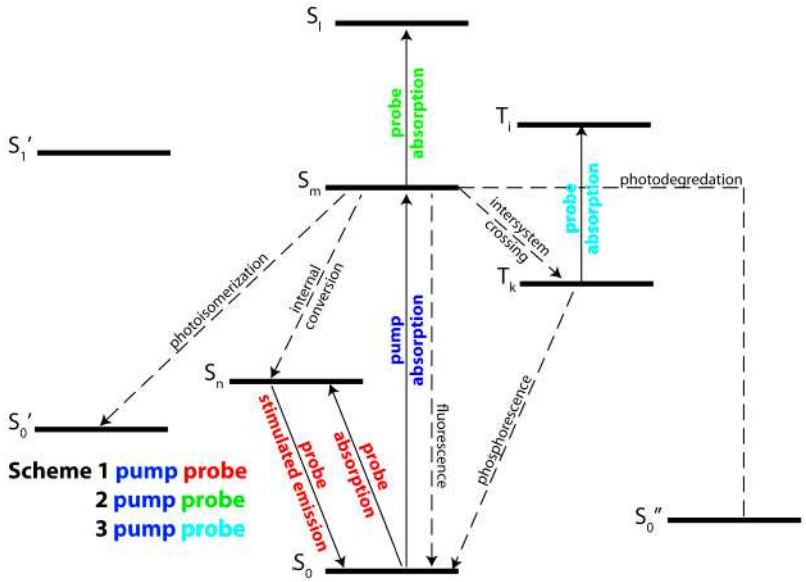

Fig. 1. Representative biomolecular energy level diagram illustrating some of the potential physical processes as well as how pump-probe spectroscopy might interrogate them. The solid arrows represent driven transitions either by the pump (blue) or probe (red, green, and cyan). The dashed arrows represent spontaneous transitions.

which lead to a new molecular species (photoisomerization and photodegredation) and others which merely change state populations (internal conversion, intersystem crossing, fluorescence, and phosphorescence). The solid lines indicate transitions that would be driven by the pump or probe radiation in three different illustrative schemes for a two-color pump-probe experiment. For all three schemes the pump drives the S_0-S_m transition. Under the assumption that S_m is initially unpopulated the pump radiation is simply absorbed, thereby driving population from the ground state (S_0) to the excited state (S_m). In scheme 1 the probe drives the S_0-S_n transition. If S_n is populated by internal conversion from S_m then the probe radiation can both be absorbed and stimulate emission when the pump is on. As a result, when the pump is on, the attenuation of the probe is lower than when the pump is off. In scheme 2 the probe drives the S_m-S_l transition. In this case the probe is only absorbed when the pump is on, hence the attenuation of the probe is higher when the pump is on than when the pump is off. Scheme 1 and 2 will produce pump-probe signals which are π out of phase with each other. Scheme 3 is similar to scheme 2 except intersystem crossing to a triplet state (T_k) follows pump excitation and the probe drives the T_k-T_i transition. Scheme 3 would have the same phase relationship as scheme 2, but likely a much longer ground state recovery time because of the forbidden transition to the ground state.

A fourth process not illustrated, but of potential importance is the internal conversion to highly excited vibrational states which leads to local heating and the emission of a pressure (acoustic) wave. We know this is an important mechanism in melanin because of its ubiquitous use as a target chromophore in photoacoustic tomography. The local heating causes small localized changes in the refractive index that have been classically detected as thermal lensing [17]. Because of the soft focusing in OCT it will not likely be sensitive to

#125174 - $15.00 USD Received 8 Mar 2010; revised 11 May 2010; accepted 14 May 2010; published 26 May 2010

thermal lensing, however OCT is inherently sensitive to changes in the refractive index because of the optical pathlength dependence of the interferometric fringes. The pressure wave may also manifest itself as a reduction in probe intensity because of phase washout due to the traveling wave. Phase washout occurs when there are phase shifts of the interferometric signal during a detector integration time thereby reducing the fringe amplitude.

The signal strength [3, 15] for schemes 1, 2, and 3 are proportional to

$$W_1 \propto \sqrt{RP_{pr}}\left(\sigma_{0,m} q_{m,n} \sigma_{0,n} N_0^0\right) P_{pu} \tag{1}$$

$$W_2 \propto \sqrt{RP_{pr}}\left(\sigma_{0,m} \sigma_{m,l} N_0^0\right) P_{pu} \tag{2}$$

and

$$W_3 \propto \sqrt{RP_{pr}}\left(\sigma_{0,m} q_{m,k} \sigma_{k,i} N_0^0\right) P_{pu} \tag{3}$$

where R is the reflectivity, P_{pr} is the probe power in the OCT interferometer, σ is the absorption cross section, $q_{m,n}$ is the quantum yield for the spontaneous transition from S_m to S_n, N_0^0 is the ground state population before interacting with the pump laser, and P_{pu} is the average pump power and assuming weak absorption (far from saturation). The square root dependence of the probe power arises because we are using interferometric detection. The probe beam and the sample arm beam in the OCT interferometer are the same, so in the standard OCT equation for signal to noise ratio, P_{pr} is equivalent to P_s.

2. System design

We have designed and assembled a two-color PPOCT system based around a Fourier domain OCT system operating at 830 nm shown schematically in Fig. 2. The OCT system utilized a tunable 140 fs Ti:Sapph laser. The Ti:Sapph was pulse- picked down to 5 MHz from its native 80 MHz repetition rate before being launched into a standard single mode fiber. Spectral broadening to 30 nm FWHM in the single mode fiber yielded an axial resolution of 11 µm. After passing through an optical delay line used to set the delay between the pump and probe the spectrally broadened beam was launched into a 2x2 (50:50) fiber coupler, which formed the Michelson

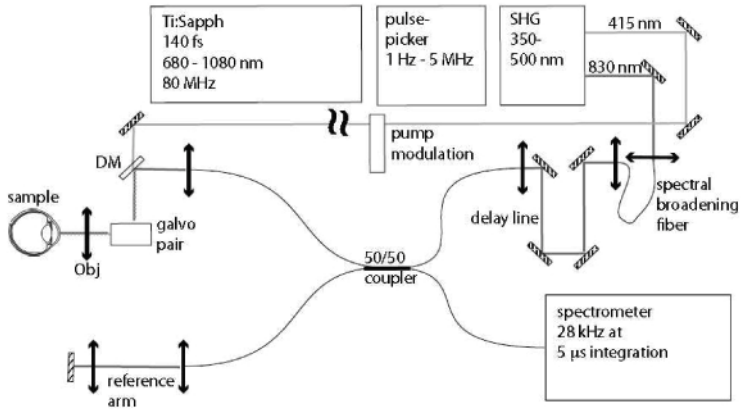

Fig. 2. Schematic diagram of the Fourier domain Pump-Probe Optical Coherence Tomography system.

interferometer. The probe pulse duration at the sample after passing through ~3 m of fiber was measured with a fast photodiode (50 ps rise time) and oscilloscope (BW = 2.5 GHz) to be 1.0 ns (FWHM). The temporal response of the detector/oscilloscope pair was measured to be 435 ps (FWHM) using the 140 fs output of the Ti:Sapph to approximate a delta function.

#125174 - $15.00 USD Received 8 Mar 2010; revised 11 May 2010; accepted 14 May 2010; published 26 May 2010

A pair of galvanometer mounted mirrors (galvo pair) scanned the beam across the sample in order to generate cross-sectional (B-scan) images and volumes. An objective (Obj) focused the pump and probe onto the sample yielding a lateral resolution of ~14 μm. A custom spectrometer was built which utilized an Atmel camera capable of line rates up to 28 kHz with a minimum integration time of 5 μs. The spectrometer had a 3 dB rolloff of ~1 mm. The measured signal to noise ratio for the OCT system for a perfect reflector in the sample arm was 102 dB (108 dB theoretical shot-noise limit) with a 50 μs integration time and 2.5 mW incident on the sample.

The frequency doubled output of the Ti:Sapph at 415 nm was used as the pump beam. The pump was amplitude modulated at 1-6 kHz by an optical chopper before being combined with the sample arm of the interferometer via a dichroic mirror (DM). The pump pulse duration was estimated to be less than 1 ps, based on the fact that the pump propagated to the sample in free space and originated from a 140 fs fundamental.

The amplitude modulation of the pump frequency encodes the PPOCT signal at the modulation frequency, f_m. In order to extract this signal we have developed the following algorithm. An OCT M-scan, was first collected and processed in the standard way, i.e. convert to k-space, resample, and inverse Fourier transform to get M(z,t). The magnitude of the processed M-scan is then Fourier transformed along the time dimension to yield M(z,f). The magnitude, |M(z,f)|, was then filtered around f_m and integrated in f to yield the PPOCT A-line P(z). Cross-sections (B-scans) were generated by collecting 3-D M-scans, M(y,z,t) and processing in a similar way to yield P(y,z).

The OCT images displayed in this article were derived in a similar fashion as the PPOCT images, except the bandpass filter was placed around DC and integrated in f. This was done in order to get the signal-to-noise ratio (SNR) advantage afforded by the multiple A-lines in each M-scan. This also ensures that the speckle is perfectly correlated between the OCT and PPOCT images and that any motion artifact affects both images the similarly.

The axial resolution in both OCT and PPOCT is a function of the coherence length of the probe, hence a broader probe spectrum leads to higher resolution. The lateral resolution in OCT is a function of the focusing of the probe onto the sample. The lateral resolution in PPOCT is a function of *both* the probe and pump focusing. The pump dependence arises from the fact that the pump and probe must overlap in order for a pump-probe signal to be generated. In our current system we have a pump at 415 nm and a probe at 830 nm. We have carefully maintained a factor of two difference between the diameter of the collimated pump and probe beams in order to ensure that the two beam waists were approximately equivalent after passing through the objective. Maximizing the overlap also maximizes the pump-probe signal.

3. Results and discussion

A series of experiments have been conducted to characterize the designed PPOCT system. These experiments were carried out on a tissue phantom constructed by embedding a black human hair (diameter ~110 μm) in chicken breast tissue. The hair was embedded at an angle relative to the tissue surface to enable continuous variation in the hair tissue depth. Black hair in particular contains eumelanin. Eumelanin is also found in the eye and skin.

Figure 3 is a series of OCT and PPOCT cross-sections recorded with the hair at various depths in the chicken breast. The pump was modulated at 6 kHz. The average power of the pump and probe was 2.2 and 2.5 mW, respectively, with the pump leading the probe by 280+/− 40 ps. The line rate was 12.2 kHz with a 50 μs integration time. The label above each column corresponds to the tissue depth of the

#125174 - $15.00 USD Received 8 Mar 2010; revised 11 May 2010; accepted 14 May 2010; published 26 May 2010

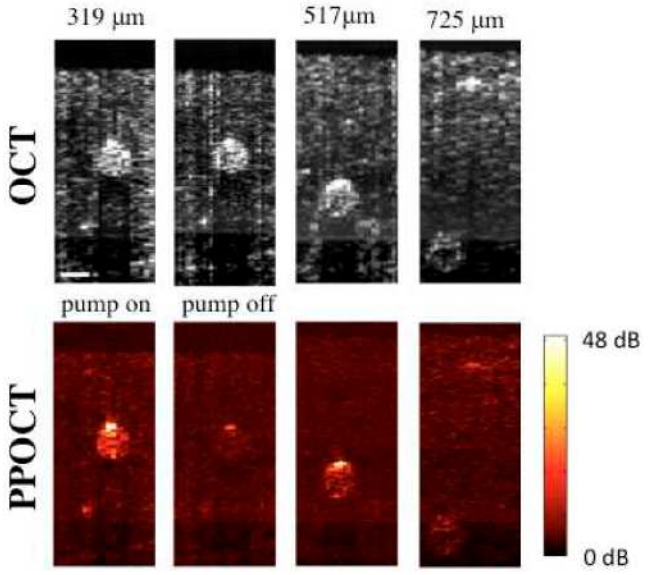

Fig. 3. PPOCT and OCT images of a human hair embedded in chicken breast at various depths in the tissue. The depth corresponds to the center of the hair. The scale bar is 100 μm. For the 315 mm depth both pump on and pump off images are shown while only pump on images are shown for other depths. The color scale bar to the right is the signal to noise ratio in dB for the PPOCT images. All images are on a log intensity scale.

center of the hair. The 319 μm image was generated using 500 OCT lines per PPOCT A-line. All others used 1000 lines. The second image in the PPOCT row was recorded with the pump beam blocked. In order to facilitate direct comparison of the PPOCT images in Fig. 3, each image was placed on an signal (S) to noise (σ_N) dB scale (SNR = $20\log(S/\sigma_N)$. The standard deviation of the noise was calculated by finding the standard deviation of the signal above the tissue surface, which should be a good approximation to the noise floor.

The PPOCT images show strong signal from the embedded hair. Only the signal from the hair is pump dependent, as evidenced by the pump blocked image. The residual signal when the pump is blocked is due to intensity noise in the laser source at the pump modulation frequency.

The hair was visible in the PPOCT image at the largest depth measured, 725 μm center depth and 780 μm maximum depth. The PPOCT signal should be more strongly attenuated as a function of depth than the OCT signal because of the much stronger attenuation of 415 nm light in tissue than 830 nm light. The images in Fig. 3 appear to be in qualitative agreement with the expected trend. Ultimately the choice of pump wavelength is a trade-off between absorption cross-section of the target chromophore and tissue scattering.

Figure 4 is a plot of OCT, PPOCT, and PPOCT background (pump off) A-lines corresponding to the center of the hair in the 319 μm images. All three A-lines have been placed on an absolute SNR dB scale in order to facilitate a quantitative comparison of signal strengths. At the tissue surface indicated by the left most arrow the OCT, PPOCT, and PPOCT background SNR was 38 dB, −4 dB and 12 dB, respectively. While there is a fairly strong OCT signal, the PPOCT and PPOCT background signals are very near the noise floor. At the peak signal in the hair indicated by the right most arrow the OCT, PPOCT, and PPOCT background SNR was 63 dB, 49 dB, and 29 dB, respectively. If we subtract the PPOCT background from the PPOCT signal we find that there is 20 dB of background free PPOCT signal. The OCT signal is 43 dB stronger than the background free PPOCT signal.

#125174 - $15.00 USD Received 8 Mar 2010; revised 11 May 2010; accepted 14 May 2010; published 26 May 2010

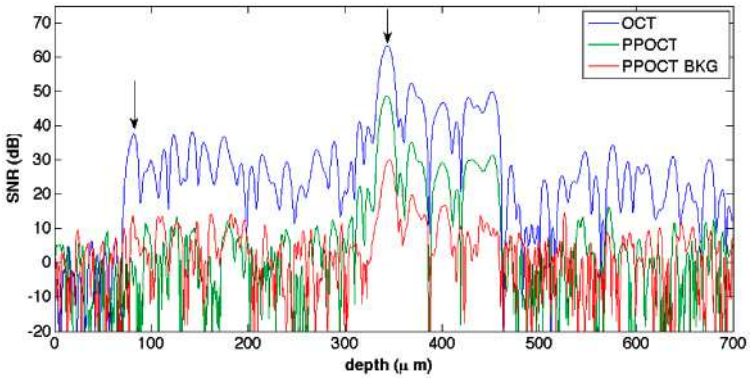

Fig. 4. OCT (blue), PPOCT (green) and PPOCT background (red) A-lines on an SNR dB scale. The A-lines were taken from the 319 μm B-scans. The PPOCT background corresponds to the pump off image.

The series of images in Fig. 5 were generated using a single data set (319 μm depth, Fig. 3). Images in each column utilize a different number of OCT lines/PPOCT A-line thereby changing the effective PPOCT A-line rate. The columns are labeled with the effective line rate, 24.4 Hz, 244 Hz, 1220 Hz, and 2440 Hz which correspond to 500, 50, 25, 10, and 5 OCT lines/PPOCT A-line. At 50 A-lines per image in Fig. 5, the total acquisition time varies from 2 s to 20 ms. While we clearly loose signal to noise at high line rates we are able, with the current system, to measure PPOCT images at line rates exceeding 1 kHz. This represents a more than 1000 fold improvement over the previous time-domain system.

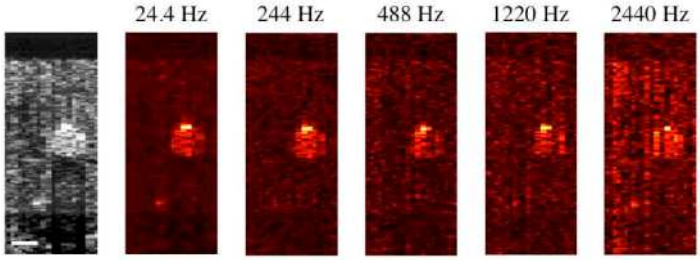

Fig. 5. OCT (grayscale) and PPOCT B-scans of a human hair embedded in chicken breast, recorded at different PPOCT line rates. In all cases the OCT line rate was 12.2 kHz, hence 24.4 Hz corresponds to 500 OCT lines/ PPOCT line. The scale bar is 100 μm. All images are on a log intensity scale.

We have also investigated the pump power and modulation frequency dependence of the signal in the range of 0.1-2.7 mW average power and 1-6 kHz, respectively, using a black human hair as a sample. Each point in Fig. 6 represents the integrated signal in a PPOCT B-scan of a black human hair divided by the integrated signal of the OCT B-scan. This algorithm was developed to improve the repeatability of the measurements (estimated at +/– 5%). The power dependence in panel A remains linear up to ~700 μW. The curvature after 700 μW indicates that we are approaching saturation of the state(s) responsible for generating the PPOCT signal. Average pump powers beyond ~3 mW will not substantially improve the SNR. Since the saturation intensity is independent of chromophore concentration these measurements may be used as a guide for imaging other eumelanin containing tissues with this system, e.g. the retinal pigment epithelium and iris.

#125174 - $15.00 USD Received 8 Mar 2010; revised 11 May 2010; accepted 14 May 2010; published 26 May 2010

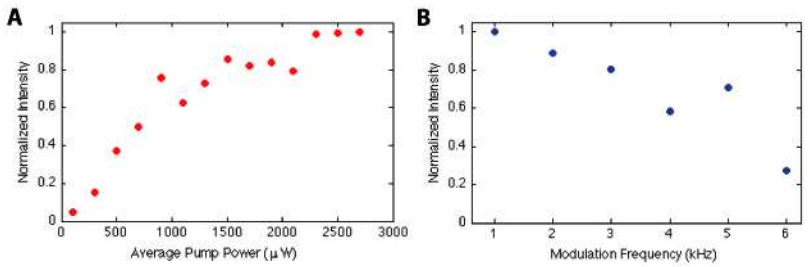

Fig. 6. A) Pump power dependence of the PPOCT signal measured with a black (eumelanin) human hair sample. B) Pump amplitude modulation frequency dependence of the PPOCT signal from a similar sample. The estimated error is ± 5%

The signal strength in Fig. 6B visibly begins to drop off (10%) starting at 2 kHz. It continues its downward trend up to the highest frequency measured, 6 kHz, where the signal is down by ~70% from its maximum. The pump induced signal clearly has a long lived component that persists on the order of several hundred microseconds. If the signal was entirely due to transient absorption from allowed transitions (scheme 2) the chromophore should completely relax between pump pulse trains and therefore not be a function of the pump modulation frequency. This does not preclude the existence of short lived states which could also contribute to the pump induced signal. If the long lived component proves to be the dominant source of pump-probe signal, it may be possible to replace the 5 MHz Ti:Sapph laser with a continuous wave source. In general, continuous wave sources are less expensive, smaller, and more robust than the femtosecond laser used in this study; all properties that would be helpful in any effort to transfer this technology to a clinical environment.

Given the complexity and uncertainty of the melanin excited state manifold, it is not obvious *a priori* what specific mechanism or mechanisms are responsible for the pump-probe signal, i.e. scheme 1, scheme 2, scheme 3, and/or local heating. The phase of the PPOCT signal relative to the pump modulation can help narrow the options. We have measured the pump modulation while acquiring an OCT M-scan by directing the weak pump beam reflection from the dichroic mirror (DM in Fig. 2) into a photodiode. The camera trigger was used to synchronize the digitization of the photodiode signal. An M-scan of the hair sample was collected in this manner. The strongest reflection in the M-scan was filtered (in time) around the modulation frequency with a digital bandpass filter (600 Hz bandwidth). The photodiode signal was processed with the same filter. A comparison of the unfiltered and filtered photodiode signal indicated that there was no inherent phase shift due to the filter itself. The filtered line in the M-scan and photodiode signal from a representative data set is shown in Fig. 7 over a 4 ms time interval. The average phase difference from eight data sets was 1.1π radians with a mean standard deviation of 0.1π radians.

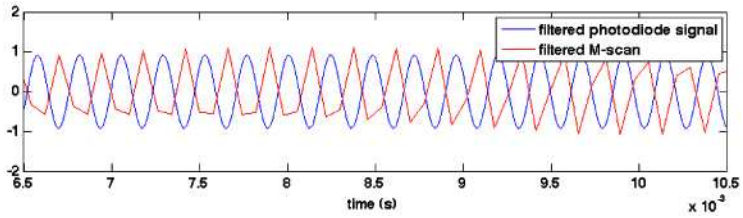

Fig. 7. Modulated pump signal (blue) and peak of the OCT M-scan (red), filtered around the pump modulation frequency.

The OCT signal amplitude is nearly perfectly out of phase with the pump, i.e. when the pump is on, the OCT signal is more strongly attenuated than when the pump is off. The π phase shift is consistent with schemes 2 and 3 and excludes scheme 1 as a significant

#125174 - $15.00 USD Received 8 Mar 2010; revised 11 May 2010; accepted 14 May 2010; published 26 May 2010

contributor. It does not rule out the possibility that at least a portion of the signal is due to thermal effects which should have a similar phase relationship.

Signal due to thermal effects, either phase washout from the pressure (acoustic) wave or localized refractive index changes from heating, should persist over relatively long pump-probe delays because of the slow acoustic wave velocity (~1500 m/s) and slow heat dissipation. In 1 ns a pressure (acoustic) wave would travel ~1.5 μm, far less than one coherence length of the source, hence we would expect little change in signal originating from pressure wave phase washout. Similarly, a time scale of 1 ns is too short for dissipation of localized heating. Any reduction of PPOCT signal at delays of ~1 ns could then be reasonably attributed to transient absorption (schemes 2 and 3).

Since our optical delay line was not readily scanable we inserted two indexed mirrors which could easily be removed and replaced with minimal alignment in order to allow us to quickly measure signals with fixed pump-probe delays of 100 ps and 1.2 ns. A PPOCT A-line of a black human hair was recorded at both delays under similar conditions. The PPOCT signal was integrated and normalized to the integrated OCT signal. A comparison of the two delays indicated a decrease in the normalized signal of 11% at the longer delay, based upon the average of three measurements. This result is consistent with at least 11% of the signal arising from transient absorption. Furthermore, the mechanism is more likely akin to scheme 2 because the long ground state recovery times expected in scheme 3 due to the forbidden transition.

A consequence of the integrative nature of absorption is that reflections distal to the chromophore deposit in the tissue will also report on the attenuation due to the chromophore. The result should be PPOCT signal at all depths distal to the chromophore deposit. Such behavior is not evident in the images of Fig. 3, i.e. there is no apparent PPOCT signal below the depth of the hair. One explanation is the strong shadowing from the chromophore absorption masks this effect. There is clearly a shadow in the OCT image. This masking was also noted in previous work [3]. An alternative explanation arises if the PPOCT signal can be attributed to thermal effects. Since over relatively short time scales the heating should be localized to the area of the tissue containing the chromophore, PPOCT signal due to thermal effects should be localized to that tissue. Unfortunately, we do not have enough information to distinguish the precise contribution of the several physical phenomena that may contribute to the PPOCT signal. Further experimental investigation is needed.

As an initial demonstration of PPOCT in a biological sample we have chosen the porcine iris which contains eumelanin. A fresh porcine eye from a healthy domestic pig (*Sus scrofa domesticus*) was obtained from the Department of Animal Science's, E. M. Rosenthal Meat Science and Technology Center at Texas A&M University. In order to avoid the need to compensate for the refractive power of the cornea, the cornea and the aqueous humour in the anterior chamber were removed to expose the surfaces of the iris and the lens. A B-scan was recorded over a 2 mm span which included the junction of the iris and lens. Memory limitations with the custom LabVIEW ® software written to acquire PPOCT images necessitated the acquisition of the B-scan in five 400 μm sections which were merged in post processing. The data acquisition time for each segment was ~4 s. There are several vertical artifacts visible in the images of Fig. 8 due to the segmented acquisition. The incident average pump and probe power were ~2.5 mW and ~1.9 mW, respectively with a pump modulation frequency of 4.2 kHz. The integration time for the camera was set at 50 μs with a line rate of 12.5 kHz. The lateral sampling was 4 μm with 500 A-lines per M-Scan used to extract the PPOCT A-line. The pump-probe delay was set to ~120 +/− 40 ps. Figure 8 shows the OCT and corresponding PPOCT images.

The OCT B-scan image, Fig. 8A, clearly depicts the iris and lens. The corresponding PPOCT image, Fig. 8B, shows a strong signal from the iris, a melanin rich region, and weak (background) signal from the lens. A B-scan recorded without the pump, Fig. 8C, showed similar signal strength from the lens. We may generate a background subtracted image by

#125174 - $15.00 USD Received 8 Mar 2010; revised 11 May 2010; accepted 14 May 2010; published 26 May 2010

subtracting 8C from 8B. Since the speckle is not correlated between Fig. 8B and 8C (there was a short delay between acquiring the two images), before making the subtraction we had to reduce the speckle by spatially averaging (16 μm x 33 μm) both images. The subtracted image is in Fig. 8D. The maximum SNR went up even though we are subtracting signal because of the spatial averaging. The background subtraction is not perfect, however in many areas where there should not be a PPOCT signal (around the lens) the background is completely removed. The maximum SNR of the lens signal stayed approximately constant between 8C and 8D, but the SNR of the iris went up by approximately 5 dB.

The OCT image is essentially a measure of the depth dependent reflectivity. The PPOCT image bears the same reflectivity information except as a product with the molecular dependent part of the signal (See Eqs. (1), (2), and (3)). We can therefore create a molecular image that is independent of the tissue reflectivity by taking the ratio PPOCT/OCT. The ratio image in Fig. 8E was calculated via the following algorithm: The OCT image was spatial averaged to match the subtracted PPOCT image and normalized. The background subtracted PPOCT image (8D) was normalized and then thresholded at 4.0% of the maximum to avoid taking the ratio of noise. The resulting image is displayed on a false color scale where black is zero

#125174 - $15.00 USD Received 8 Mar 2010; revised 11 May 2010; accepted 14 May 2010; published 26 May 2010

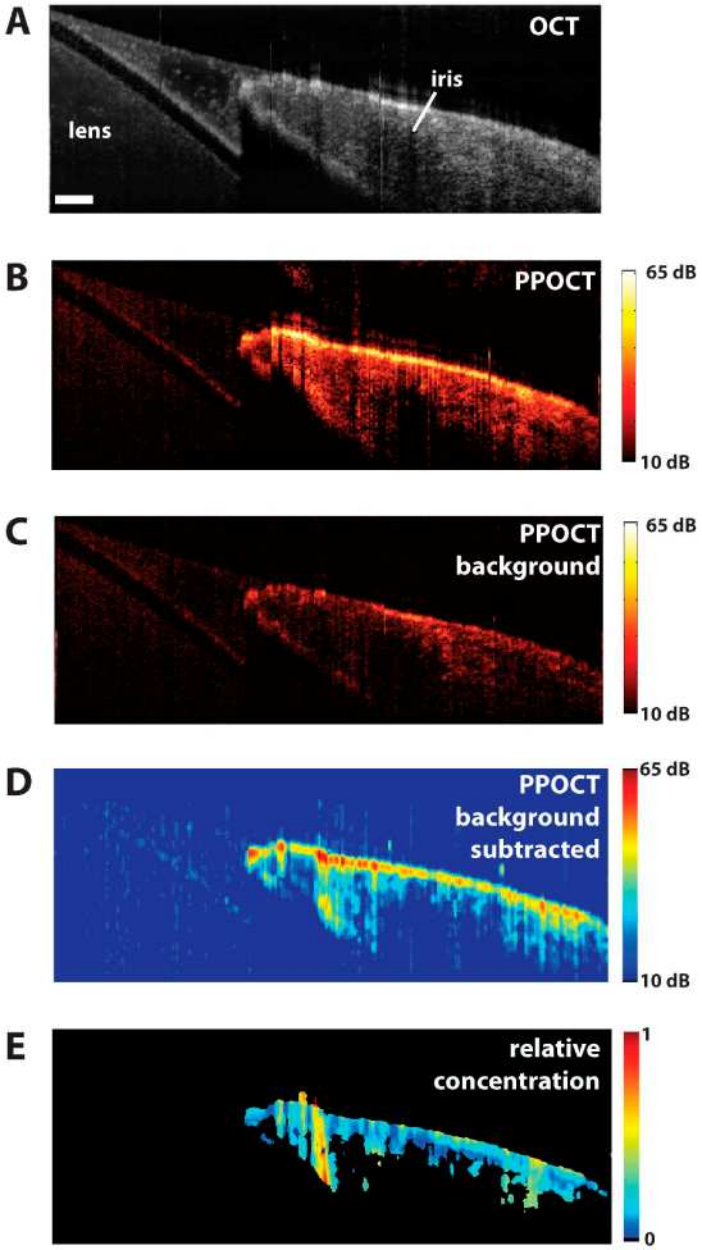

Fig. 8. A) OCT image of the porcine lens and iris. The scale bar is 200 μm. B) PPOCT image mapping the melanin in the iris. The color bar is in dB SNR. C) PPOCT background image recorded without the pump radiation. The color bar is in dB SNR. D) Background subtracted PPOCT image derived from spatially averaged version of B and C. The color bar is in dB SNR. E) Reflectivity independent molecular image on a linear scale where 1 indicates the maximum concentration. All images except E are on a log scale.

(thresholded) and above zero to 1 varies from blue to red. The ratio image is displayed on a linear intensity scale, in contrast to the other images which are displayed on a log intensity scale. It is interesting to note that the strong iridial surface signal in the PPOCT image is no longer the dominant signal in the ratio image. The signal in the ratio image is a much weaker function of depth.

#125174 - $15.00 USD Received 8 Mar 2010; revised 11 May 2010; accepted 14 May 2010; published 26 May 2010

A potential application of this technology is imaging melanoma in the iris and retinal pigment epithelium. Melanoma is the most common form of adult ocular cancer which originates in the melanin producing melanocytes. In order to image melanin in the eye we must adhere to the ANSI limits for ocular exposure. OCT is typically performed at or below 600 μW (@ 800 nm) which is safe for continuous viewing. The pump laser need only illuminate the eye after an initial OCT scan to choose the area of interest, hence the dwell time for the pump laser may be relatively short. If we assume we are able to acquire a suitable number of images for diagnosis in 1-10 s the maximum permissible exposure at the pump wavelength (415 nm) is 692 μW for a 1 s exposure and 390 μW for a 10 s exposure. Based on Fig. 6A we would expect a PPOCT signal reduction of 50-80% based on the pump power reduction. This reduction could likely be compensated by system improvements such as a faster spectrometer. The imaging speed would also need to be improved or a retinal tracking system incorporated in order to avoid the motion artifact endemic to *in vivo* imaging of the eye. The blue edge of the visible spectrum has poor ocular transmission [18], hence the pump would also likely need to be moved to longer wavelengths in order to make it feasible to image the living iris and retina. We have moved the pump to 450 nm (same ANSI limits) with no significant drop in the PPOCT signal. Longer wavelengths were not possible at equivalent power with our current laser system. We believe that with system improvements and a longer pump wavelength it would be possible to image the living iris and retina.

Conclusions

We have designed and built the first two-color Fourier domain Pump-Probe Optical Coherence Tomography system. The system was characterized using a contrived tissue sample consisting of a black (eumelanin) human hair embedded in chicken breast. The imaging depth of the PPOCT system was shown to be nearly comparable to the base OCT system and confirmed to be greater than 725 μm in chicken breast tissue. Similar experiments showed that PPOCT A-line rates up to 2.4 kHz were possible in tissue albeit at reduced signal to noise. Measurements of the pump power dependence of the signal showed that the signal is approaching saturation beyond ~700 μW, hence high powers will produce diminishing returns in PPOCT signal strength. Investigation of the pump modulation frequency dependence of the PPOCT signal indicated a steady deterioration of the signal at increasing pump modulation frequency. This dependence was interpreted as evidence for long lived components in the PPOCT signal. Further experiments aimed at revealing the physical origin of the PPOCT signal provided evidence for short lived components as well, which were attributed to transient absorption. The precise contribution of transient absorption and thermal effects to the long lived component could not be ascertained. The potential for imaging melanin in the eye was demonstrated by *ex vivo* imaging of the porcine iris.

Acknowledgements

We gratefully acknowledge support for this work through a grant from the National Institutes of Health, R21EB007729.

#125174 - $15.00 USD Received 8 Mar 2010; revised 11 May 2010; accepted 14 May 2010; published 26 May 2010